MDPI

Article

Analysis of the Influence of Thermophysical Properties of a Droplet Liquid on the Work Processes of a Two-Stage Piston Hybrid Power Machine

Victor Shcherba [1],*, Evgeniy Pavlyuchenko [1], Evgeniy Nosov [1] and Irina Bulgakova [2]

[1] Hydromechanics and Machines Department, Omsk State Technical University, 644050 Omsk, Russia; eapavlyuchenko@omgtu.ru or hystonru@mail.ru (E.P.); eyunosov@omgtu.ru (E.N.)

[2] Foreign Languages Department, Omsk State Technical University, 644050 Omsk, Russia; bulgakova-i@mail.ru

* Correspondence: scherba_v_e@list.ru or vesherba@omgtu.ru; Tel.: +7-3812-65-31-77

Abstract: The article considers the influence of the main thermophysical properties of the power liquid on the working processes and energy characteristics of a new highly efficient two-stage piston hybrid power machine designed to compress gas to medium and high pressures. Mathematical model of the working processes of the machine under study with a pro-filed working chamber of stage 2 has been developed. To verify the developed mathematical model of working processes, a prototype and a stand for its study were created. The visualization of the movement of the liquid piston, measurement of the instant pressure in the working chamber of the machine, energy and consumption characteristics verified the developed mathematical model. As a result of a numerical experiment, we determined that there is an optimal value of the dynamic viscosity of the power liquid, which depends on the angular velocity of the crankshaft and is in the range from 0.005 to 0.02 Pa·s, with large values referring to large values of the angular velocity. With a decrease in the density of the power liquid, the work of friction forces decreases and the total indicator efficiency increases. The findings of the research can be used when choosing coolants in reciprocating compressors with a liquid piston.

Keywords: piston hybrid power machine; liquid piston; liquid viscosity; liquid density; high pressure compressed gas

1. Introduction

The ever-growing demand for new technology prototypes stimulates the development of research and development works, mostly in energy-intensive branches of technology. These branches include pump and compressor construction. More than 20% of the power used is spent on the drive of pumping units [1,2]. As a result, the task of increasing the efficiency of recently produced pumping and compressor units is important and urgent.

An increase in the total efficiency of a piston compressor is connected with an increase in indicator efficiency, mechanical efficiency, and transmission efficiency. Indicator efficiency can be increased in the following ways: by developing the cooling of the compressed gas [2], a decrease in the leakage of the compressed gas through the leaks of the cylinder-piston group and valves [3–5], a decrease in losses of work in suction and discharge by reducing the gas and valve closure oscillations [3–5]. An increase in the displacement ratio of a reciprocating compressor is due to a decrease in the leakage of the compressed gas, a decrease in dead space, and an increase in the density of the intake gas due to an increase in pressure (resonant or mechanical boost), as well as a decrease in the temperature of the intake gas [6]. It should be noted that the most in the indicator efficiency can be achieved by approaching compression to isothermal by intensive cooling of the compressed gas [7,8]. Currently, there are three main types of cooling used in compressors: air, water and coolant injection.

From a thermodynamic point of view, the coolant injection is the most efficient due to the developed heat exchange surface and absence of thermal resistance between the compressed gas and the coolant [9,10]. However, significant energy costs connected with liquid spraying and its separation, as well as operational difficulties, significantly slow down the widespread introduction of this type of cooling.

Air cooling is simple for practical implementation, however, due to its low efficiency, mostly it is used in general-purpose compressors with a discharge pressure of up to 1.0 MPa of low capacity.

The majority of medium and high pressure piston compressors of small, medium, and high capacity are water-cooled [11].

As a result, the idea of combining a piston compressor and a piston pump into a single unit called the "piston hybrid power machine" (PHPM) appeared. The schematic diagram of the cross-head PHPM is shown in Figure 1.
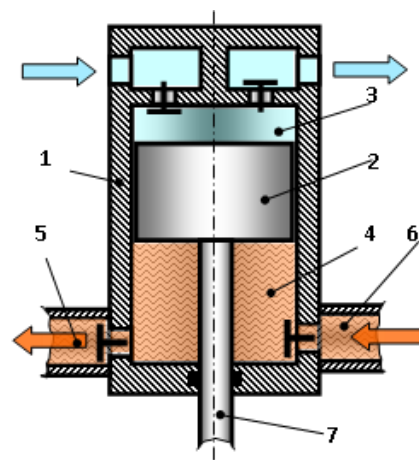

Figure 1. Construction diagram of PHPM (1—cylinder; 2—piston; 3, 4—compressor and pump cavity; 5, 6—discharge and suction liquid nozzles; 7—plunger).

The PHPM upper part is the compressor section, and the PHPM lower part is the pumping section. One piston is used to compress and move gas and liquid; there is liquid in the gap between the piston and the cylinder, which eliminates the leakage of the compressed gas. In the first case, the pumping section can be independent and be considered a pump for pumping liquid. In this case, the compressor is cooled along the way without energy costs. In the second case, the pumping section can be considered a pump for pumping liquid through the cooling jacket. Then, the cost of driving the pump section must be added to the cost of energy to drive the compressor.

When combining the pump and compressor into a single unit, we achieve intensive cooling of the compressed gas, elimination of leaks in the cylinder–piston group, significant reduction or elimination of dead space, and reduction of friction forces in the cylinder–piston group due to the regulation of liquid friction.

All the aspects result in improved performance and overall compressor efficiency.

Combining with a compressor is useful for a pump. When combined, the suction cavitation margin increased due to the flow of liquid from the gap in the cylinder–piston group; the work supplied in the cycle decreases due to the utilization of the compressed gas heat [12].

Multistage reciprocating compressors are used to compress gas to medium and high pressures. The number of stages varies from 3 to 4, depending on the type of cooling. When using air cooling, the degree of pressure increase in the stage is within 5–6, and when using water cooling, it can be increased to 10–12. When using coolant injection, its value can be raised up to 20, even for gases with a high adiabatic index, such as helium.

One of the promising schemes for multistage gas compression to high pressures is its preliminary compression in a reciprocating compressor and final compression in the cylinder using a liquid piston [13,14].

The use of a liquid piston regulates its intensive cooling, eliminates leaks in the cylinder-piston group, and the size of the dead space. These factors lead to an increase in the indicator efficiency and the compressor delivery ratio.

Thus, this gas compression scheme needs a compressor for preliminary gas compression and a pump for its final compression. This condition is satisfied by the two-stage PHPM shown in Figure 2. The PHPM stage 1 is a single-stage crosshead power machine with piston 1 located in cylinder 2. Piston 1 divides the working volume of cylinder 2 into compressor chamber 5 and pump chamber 13. The pumping chamber is connected by pipeline 14 with stage 2 of the machine, which has liquid volume 16 (liquid piston) and gas volume 17.
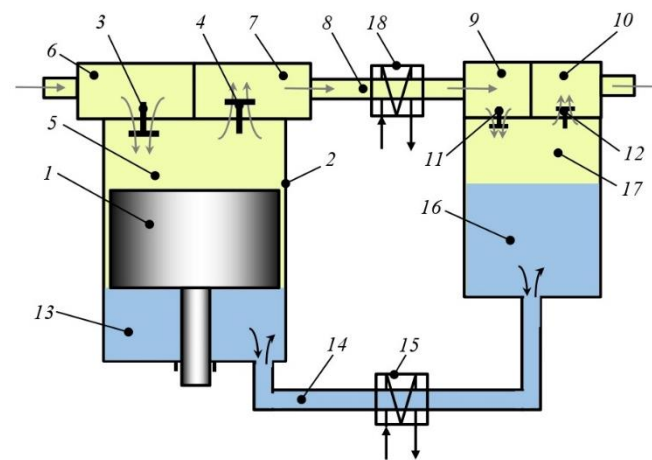

Figure 2. Schematic diagram of a two-stage PHPM without a cylinder cap.

The compressor section of stage 1 has suction chamber 6 and discharge chamber 7 connected through suction valve 3 and discharge valve 4 to working chamber 5. The discharge chamber 7 of stage 1 is connected by pipeline 8 to suction chamber 9 of stage 2. Suction chamber 9 is connected by suction valve 11 of stage 2 of the compressor section to working chamber 17, and the latter is connected to the pressure chamber of stage 2 by pressure valve 12. Compressed gas is supplied from discharge chamber 10. There are heat exchangers 15 and 18 to remove heat from the preliminary compressed gas and the power liquid.

The two-stage PHPM works as follows: During the upward stroke of piston 1, gas is compressed and pumped from working chamber 5 through discharge valve 4 into pumping chamber 7. At the same time, pumping chamber 13 increases and the liquid from chamber 16 of stage 2 enters chamber 13 through connecting pipeline 14. The preliminary compressed gas enters suction chamber 9 through connecting pipeline 8, and through suction valve 11 enters gas chamber 17 of stage 2, where the gas pressure decreases.

During the downward stroke of piston 1, gas is sucked from suction chamber 6 through suction valve 3 into working chamber 5. The volume of pumping chamber 13 decreases, thus the liquid enters chamber 16 through pipeline 14, its volume increases, and volume of gas chamber 17 decreases.

A decrease in chamber 17 leads to an increase in its pressure. When the discharge pressure is reached, discharge valve 12 opens and gas enters discharge chamber 10.

When liquid in the pumping section of stage 1 exceeds the volume of the working chamber of stage 2, the excess liquid enters the gas cap installed on the connecting pipeline. In the considered machine, there is no gas cap and the volume of stage 1 pumping section is equal to the working volume in stage 2 compressor section.

Thus, the two-stage PHPM provides intensive cooling in stages 1 and 2, elimination of leaks in their cylinder-piston groups, elimination of dead space in the stages of the machine, which provides a high indicator efficiency and compressor delivery coefficient at high weight and dimensional characteristics.

Completed works on the study of reciprocating compressors with a liquid piston [15–17] were aimed at studying the processes of heat transfer and its effect on the compression efficiency. In [18], we analyzed the effect of inserts from a porous medium on the operation of a liquid reciprocating compressor. The influence of the speed of the liquid piston on the working processes of the compressor was studied in [19]. The authors of [20] considered the influence of the main size and operational parameters on the dynamics of liquid movement and work processes in a reciprocating compressor with a liquid piston.

The references review shows that mostly the influence of size, operational, and thermal parameters on the operation of a liquid piston was studied. However, studies on the influence of the main thermophysical properties of a liquid on the dynamics of the movement of a liquid piston could not be found.

A significant influence on the dynamics of the motion of a droplet liquid, which ensures gas compression in stage 2 of the compressor, is exerted by its main thermophysical properties: density, viscosity, coefficient of volumetric compression, and coefficient of thermal expansion. Taking into account that the effective pressure drop on the liquid is not more than 10 MPa, and the modulus of elasticity of the droplet liquids is about 2000 MPa, the effect of the compressibility of the liquid on the working processes in the machine can be neglected. The performed theoretical studies established that, in the range of the investigated pressures (up to 15 MPa), the compressibility of a liquid in a two-stage PHPM under the action of gas forces, inertial forces, and resistance forces does not exceed 1%, and the decrease in the instant velocity of the liquid piston is within 5%. Thus, we assume that the liquid is incompressible.

It should be noted that the temperature coefficient β_T for dripping liquids is higher than the volumetric compression ratio β_p, but its absolute value remains small. So, for water, it is 0.63×10^{-4} K^{-1}. It should be noted that low absolute β_p and β_T even if they are changed several times will not have a significant effect on the working processes of the machine.

The density ρ_w and the dynamic viscosity of the liquid μ_w are different. Values ρ_w and μ_w change significantly both when changing thermodynamic parameters, primarily temperature, and when using various liquids. So, for example, the dynamic viscosity of water at $T = 293$K is $\mu_w = 1004 \times 10^{-3}$ Pa·s, but the dynamic viscosity of industrial oil M-20A at $T = 313$K is $\mu_w = 26.7 \times 10^{-3}$ Pa·s, i.e., 26 times greater. We observe similar trends with the density of the liquid.

This research is devoted to the analysis of the influence of the density and viscosity of the working fluid on the working processes and integral characteristics (indicative power and pressure loss in connecting communications) of a two-stage PHPM. The issue of designing and manufacturing a prototype of a piston hybrid power machine with a liquid piston, designed to compress gas to medium and high pressures, is considered; the physical picture of the working processes in the machine under study is studied. With the developed mathematical model of the working processes of the prototype, the influence of the main thermophysical properties of the working fluid: dynamic viscosity and density on the working processes and energy characteristics of the new two-stage PHPM will be considered.

2. Theoretical Research

2.1. Determination of Basic Geometric Parameters

For a given capacity and number of revolutions, using well-known techniques [11], the diameter of stage 1 piston, stage 1 piston stroke, the main parameters of the self-acting valves, and the diameters of the interstage pipelines are determined. In our case, we coordinate the operation of stage 1 of the pump section and stage 2 of the compressor

section. In this case, we determine the volume of the working chamber of stage 2 of the compressor section and the diameter of the stem in the pump section. In addition, to improve the operation of stage 2 of the PHPM, profiling the working chamber has been completed.

2.1.1. Determination of Working Chamber of Stage 2

We determine the amount of intake gas into stage 2 of the compressor, neglecting leaks and overflows of gas in stage 1 of the compressor, from the equality of the masses of gas entering stages 1 and 2. Assuming that the compressible gas follows the laws of an ideal gas, we obtain:

$$V_{sc2} = V_{sc1} \frac{T_{sc2}}{T_{sc1}} \frac{P_{sc1}}{P_{sc2}} \tag{1}$$

Considering that $V_{sc1} = V_{h1}/\lambda_1$, but $V_{sc2} = V_{h2}/\lambda_2$ Equation (1) is transformed to:

$$V_{h2} = V_{h1} \frac{\lambda_2}{\lambda_1} \frac{T_{sc2}}{T_{sc1}} \frac{P_{sc1}}{P_{sc2}} \tag{2}$$

Values T_{sc2} and P_{sc2} can be determined as $T_{sc2} = T_{sc1} + \Delta T_{H0}$, $P_{sc2} = P_{D1} - \Delta P_c$. In view of the above, Equation (2) is transformed to:

$$V_{h2} = V_{h1} \frac{\lambda_2}{\lambda_1} \left(1 + \frac{\Delta T_{HO}}{T_{sc1}} \right) \left(\frac{1}{\varepsilon_1 - \frac{\Delta P_c}{P_{sc1}}} \right) \tag{3}$$

Values λ_1, λ_2 and ΔT_{H0}, ΔP_c are determined on well-known recommendations [11].

The working volume of the pumping section of stage 1 V_{cp1} equals to the working volume of stage 2. Thus, the rod diameter is determined as:

$$d_r = \sqrt{d_1^2 - \frac{4 V_{h2}}{\pi S_{h1}}} \tag{4}$$

2.1.2. Profiling of Stage 2 Working Chamber

When designing and operating compressor units with a liquid piston, a number of measures are used to improve the kinematics and integrity of the liquid piston by reducing foaming, crushing, and carrying part of the liquid through the discharge valve out.

For this purpose, the compressor chamber is profiled (the working chamber of stage 2 of the PHPM compressor section) and devices for stabilizing the movement of liquid of various designs are used, for example, made in the form of movable and stationary permeable solid inserts and elements.

The main reason for the liquid piston destruction is the effect on the liquid of inertial forces caused by the acceleration of the pump piston supplying liquid to the working chamber. In order to reduce inertial forces, it is necessary to bring the liquid velocity in the working chamber closer to a certain constant value, for example, the average piston speed in the pump.

To achieve this goal, it is necessary to profile the working chamber, i.e., change the flow area (F) along the length of the working chamber (S).

Currently, various profiling techniques have been developed based on different optimization criteria or their combination [21]. In practice, it is advisable to use working chambers obtained using simple bodies of revolution: a cylinder and a cone (see Figure 3).

In [21], after analyzing the working processes and operating features of stage 2 of the high-pressure compressor, it was proposed to replace the cylindrical chamber (position "a" Figure 3) with a combined one (position "b" Figure 3) having two conical parts and one cylindrical. Conducted theoretical studies [21] established that the working chamber, consisting of two truncated cones, provides a high heat exchange surface, good stabilization of the liquid piston speed with high ergonomic parameters.
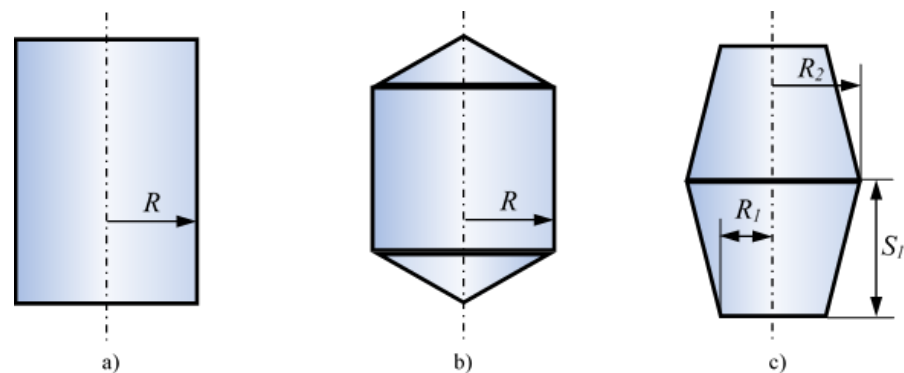
Figure 3. Different profiles of the working chambers of stage 2 of the PHPM ((**a**)—cylindrical; (**b**)—combined, made up of cones and cylinders; (**c**)—combined, made up of two truncated cones).

Considering the above, we use the working chamber of stage 2 consisting of two truncated cones (see Figure 3, position "c"), its working volume can be determined as:

$$V_{h2} = 2S_1 \frac{1}{3}\pi \left[R_1^2 + R_1 \cdot R_2 + R_2^2 \right] \tag{5}$$

The ratio of the height of the cone to the diameter of its base, in accordance with [15] is to be chosen in the range from 10 to 20.

2.2. Review of Mathematical Models and System of Accepted Assumptions

The two-stage piston hybrid power machine has stages 1 and 2 of compression and inter-stage connections for gas and liquid. Stage 1 of the investigated machine is a single-stage piston hybrid power machine. In [22], the mathematical model of working processes of a cross-head PHPM with a smooth seal is considered for the first time. The works [13,23] are devoted to the development of a mathematical model of the working processes of a cross-head PHPM with a gas chamber in the pump section. In these works, the simultaneous compression of liquid and gas in the working processes of a piston pump was considered for the first time.

The developed mathematical models are based on the following basic equations:

- for the chambers of the compressor section: the first law of thermodynamics of a body of variable mass, the equation of conservation of mass, the equation of volume change, the equation of state, the equation of the dynamics of motion of the closure body of the self-acting valve;
- for the working chamber of the pump section: the energy conservation equation written in the form of the Bernoulli equation; Hooke's equation, volume conservation equation, mass conservation equation. In [24,25], a general approach was developed for calculating work processes in the working chamber of a compressor and a positive displacement pump.

It should be noted that the developed models simulate the working processes in the compressor section, pump section, piston seal, as well as the flow of gas and liquid in the connecting pipelines.

When calculating the gas flow in the connecting pipelines of the compressors, we use a system of equations including the continuity equation, the equation of motion, and the equation for the conservation of internal and kinetic energy. The equation of state for an ideal gas is used as the equation of state. One of the effective methods for the numerical solution of such a system of partial differential equations as for single-phase flow or two-phase flow is the "large particles" method [7].

Currently, when modeling work processes in machine chambers, both distributed-parameter and lumped-parameter models are used. Taking into account the small linear dimensions of the working chambers of the displacement machines [11], as well as signifi-

cant mathematical difficulties and implementation time, the researchers use models with lumped parameters. As a result, the use of mathematical models with lumped parameters in the above works is verified and useful. It seems reasonable to use a mathematical model with lumped parameters when developing a mathematical model of a two-stage PHPM.

When considering the flow of gas and liquid in the connecting pipes of the machine, a one-dimensional flow is considered either in an unsteady or in a quasi-stationary setting [26]. If the pipeline is simple, without local resistance, and a mathematical model with distributed parameters is used to describe the working processes, we use a non-stationary one-dimensional flow model. If there are complex pipelines with closure and control valves, as well as when using a mathematical model with lumped parameters to describe thermogasdynamic processes in machine chambers, we use a quasi-stationary model for calculating the flow of gas and liquid in connecting pipes.

System of accepted basic assumptions:

- taking into account the above, we accept a mathematical model with lumped parameters to simulate the working processes of a two-stage PHPM;
- taking into account that the mathematical models of the working processes of single-stage cross-head and crosshead-free PHPMs are well developed, we consider the working processes in stage 2 of the PHPM and the liquid movement from the pump section of stage 1 through the connecting pipeline to stage 2;
- the thermodynamic gas parameters in stage 2 suction chamber are constant and equal to their rated values;
- the motion of the liquid at each moment of time is steady and stationary, i.e., the motion of the liquid is quasi-stationary;
- the working liquid has constant temperature and follows Newton's laws;
- the thermophysical properties of the liquid are constant;
- coefficients of friction along the length and local coefficients of resistance obtained for stationary conditions are also valid for unsteady flow;
- the bottom of the liquid piston is a plane parallel to the ground;
- there is no droplet liquid in the compressed gas in stage 2 of the PHPM;
- compressed gas follows the laws that are true for an ideal gas;
- the simulated processes in a compressible gas are equilibrium and reversible;
- the change in kinetic and potential energy for a compressible gas can be neglected.
- the movement of the closure body of a self-acting valve is considered as the movement of a material point;
- the walls of the pipeline and working chambers are considered absolutely rigid.

2.3. Mathematical Model of the Working Processes of a Two-Stage PHPM

The working chamber of stage 2 consists of two truncated cones (see Figure 4), having the same geometric dimensions and located symmetrically about the axis passing through the center of the working chamber and perpendicular to the vector of the liquid velocity. Thus, we have a working chamber consisting of a diffuser and confuser parts, when the liquid moves in both forward and reverse directions.

The system of differential equations describing the change in the thermodynamic parameters of gas in stage 2 of the PHPM and the motion of liquid includes: the first law of thermodynamics of a variable mass body for an open thermodynamic system; the equation of conservation of mass, the dynamics of motion of the closure body of the self-acting valve, the equation of state for a compressible gas, as well as the equation of conservation of energy and the equation of continuity for the liquid phase, can be written as:

$$dU_g = dQ_g - p_g dV_g + \sum_{i=1}^{N_1} i_{ni} dM_{ni} - \sum_{i=1}^{N_2} i_0 dM_{0i} \tag{6}$$

$$dM_g = \sum_{i=1}^{N_1} dM_{ni} - \sum_{i=1}^{N_2} dM_{0i} \tag{7}$$

$$m_{rdv}\frac{d^2 h_c}{d\tau^2} = \sum F_i \tag{8}$$

$$dp_g = (k-1)\left(\frac{dU_g}{V_g} - \frac{U_g}{V_g^2}dV_g\right) \tag{9}$$

$$dT_g = \frac{1}{k}\left(p_g dV_g + V_g dp_g\right) - T_g dM_g \tag{10}$$

$$dz_w + \frac{dp_w}{\rho_w g} + d\left(\frac{v_w^2}{2g}\right) + d\left(h_l + h_\zeta + h_{in}\right) = 0 \tag{11}$$
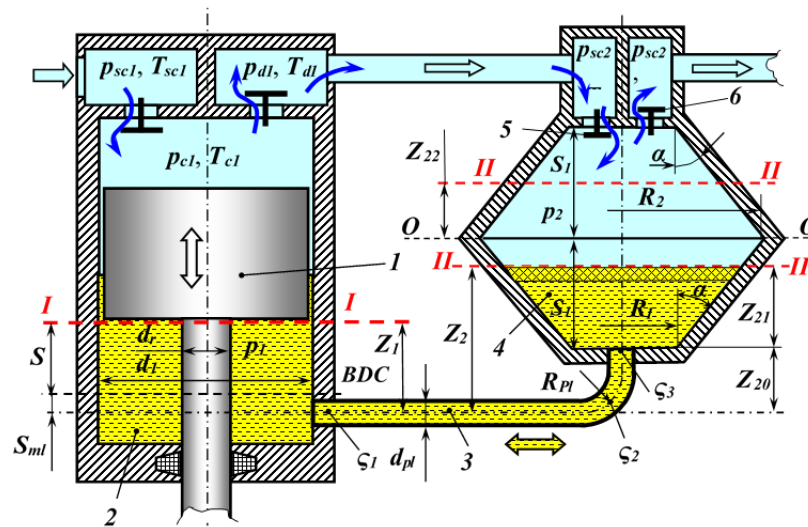
$$dQ_w = d(V_w f_w) = 0 \tag{12}$$

Figure 4. Schematic diagram of a two-stage PHPM with a profiled working chamber of stage 2.

When determining the elementary amount of heat removed from the compressed gas, the Newton–Richmann hypothesis was used:

$$dQ_g = \alpha_w \sum_{i=3}^{N_3=3} F_{ni}\left(\overline{T}_w - T_g\right)d\tau \tag{13}$$

The total heat transfer surface during gas compression can be defined as:

$$\sum_{i=1}^{N_3=3} F_{ni} = F_p + F_b + F_{vp} \tag{14}$$

Piston surface area F_p and valve plate F_{vp} can be defined as $F_p = \pi(R_1 + z_{21}tg\alpha)^2$, $F_{vp} = \pi R_1^2$.

The side surface of the working chamber (see Figure 4) can be determined as

$$F_b = \pi(R_2 + R_1)\cdot\frac{S_1}{cos\alpha} + \frac{\pi(R_2 + R_1 + z_{21}\cdot tg\alpha)(S_1 - z_{21})}{cos\alpha}$$

Heat transfer coefficient α_w, in general for a reciprocating compressor is determined on the experimental studies. In most practical cases, an empirical ratio is used to determine the heat transfer coefficient in the cylinder of a single-acting compressor $N_u = f(A, B, R_e)$ [11]. The piston speed is used as the determining speed in defining the Reynolds number. In our case, we use the average mass velocity of the liquid in the working chamber of stage 2 as the determining speed.

The average integral value of the surface temperature of the working chamber can be determined as:

$$\overline{T}_w = \frac{\overline{T}_{vp}F_{vp} + F_b\overline{T}_b + F_p \cdot \overline{T}_w}{\sum_{i=1}^{N_3} F_{ni}} \tag{15}$$

When determining the mass flows of the attached (dM_{ni}) and detached (dM_{0i}) through the gas distribution bodies, the San Venant–Wanzel equation was used for a one-dimensional isentropic flow in a quasi-stationary setting. Changing working chamber dV_g was limited by a change in the volume in the pumping section of stage 1 in the absence of dropping liquid compressibility.

When integrating Bernoulli Equation (11), two sections were used: the first section (I-I) was aligned with the lower boundary of the mechanical piston of stage 1, and the second section (II-II) was aligned with the surface of the liquid piston.

The first coordinate can be determined as:

$$z_1 = S_{ld} + \frac{S_h}{2}\left[(1 - cos\varphi) + \frac{\lambda_m}{4}(1 - cos2\varphi)\right] \tag{16}$$

The second coordinate can be determined as:

- the height of the surface of the liquid piston is less than the height of the truncated cone (S1), then $z_2 = z_{20} + z_{21}$. Value z_{21} is determined from the solution of the following nonlinear volume conservation equation

$$\frac{1}{3}\pi z_{21}\left[R_1^2 + R_1 \cdot (R_1 + z_{21}tg\alpha) + (R_1 + z_{21}tg\alpha)^2\right] = \left\{Sh - \frac{S_h}{2}\left[(1 - cos\varphi) + \frac{\lambda_m}{4}(1 - cos2\varphi)\right]\right\} \cdot F_1 \tag{17}$$

- the surface of the liquid piston is greater than the height of the truncated cone (S_1), then $z_2 = z_{20} + S_1 + z_{22}$. Value z_{22} is determined from the equation of conservation of the liquid volume

$$\frac{1}{3}\pi S_1\left(R_1^2 + R_1 \cdot R_2 + R_2^2\right) + 1/3\pi z_{22} \cdot \left[R_2^2 + R_2(R_2 - z_{22}tg\alpha) + (R_2 - z_{22}tg\alpha)\right] = \{S_h - S_h/2[(1 - cos\varphi) + \lambda_m/4(1 - cos2\varphi)]\} \cdot F_1 \tag{18}$$

The liquid velocity in the first section V_1 is determined by the kinematics of stage 1 piston drive mechanism, and the liquid velocity in the second section V_2 is determined based on the continuity equation. Total head losses consist of head losses along the length Δh_l, head loss on local resistance Δh_ζ and inertial head losses Δh_{in} ($\Delta h_\Sigma = \Delta h_l + \Delta h_\zeta + \Delta h_{in}$).

We determine the values included in the total head losses Δh_Σ.

Head losses along the length (Δh_l) are determined from the head losses along the length in the pumping chamber of stage 1, head losses along the length in pipeline 3 and head losses along the length in the profiled working chamber of stage 2 $\Delta h_l = \Delta h_{l1} + \Delta h_{lpp} + \Delta h_{l2}$.

Head losses along the length Δh_{l1} and Δh_{lpp} can be determined based on the Darcy–Weisbach law as follows $\Delta h_{l1} = \lambda_{c1}(z_1/d_1)\left(v_1^2/2g\right)$, $\Delta h_{lpp} = \lambda_{cpp}(l_{pp}/d_{pp})\left(v_{pp}^2/2g\right)$.

Length friction coefficients λ_{c1}, λ_{cpp}, λ_{c2} in general, are a function of the Reynolds number and relative roughness and is determined on the known recommendations.

The compression chamber of stage 2 consists of a diffuser and a confuser, and the head losses can be determined in them as follows:

- for the diffusor

$$\Delta h_{l2} = \frac{\lambda_{c2}}{8sin\alpha}\left(1 - \frac{1}{n_g^2}\right)\frac{v_{21}^2}{2g} \tag{19}$$

where $n_g = (R_1 + z_{21} \cdot tg\alpha)^2/R_1^2$ is diffuser expansion ratio; $v_{21} = v_1 F_1/\left(\pi R_1^2\right)$ is liquid velocity in the initial section of the diffuser.

- for the confusor

$$\Delta h_{l2} = \frac{\lambda_{c2}}{8sin\alpha}\left(1 - \frac{1}{n_K^2}\right)\frac{v_{22}^2}{2g} \tag{20}$$

where $n_k = R_2^2/(R_2 - z_{22}tg\alpha)^2$ is the degree of narrowing of the confuser; $v_{22} = v_1F_1/(\pi[R_2 - z_{22}tg\alpha])$ is liquid velocity in confuser.

The head losses on local resistances (Δh_ζ) depend on the direction of the liquid flow, as when moving forward the local resistance is a sudden narrowing, and with the reverse liquid movement—there is a sudden expansion.

As a consequence, when determining local resistances, it is necessary to take into account the direction of the piston movement.

All local resistances can be divided into four types:

- local resistance when connecting stage 1 pumping section to connecting pipeline 3—sudden narrowing (ζ_1);
- local resistance when flow turns (ζ_2);
- local resistance when connecting pipeline 3 to the working chamber of stage 2—sudden expansion (ζ_3);
- constant expansion in the diffuser part of the working chamber ζ_g and constant narrowing in the confuser part of the working chamber ζ_k.

In sudden narrowing, ζ_1 can be determined as:

$$\zeta_1 = 0.5(1 - n_\zeta) \tag{21}$$

where $n_\zeta = \omega_2/\omega_1$ is the ratio of the areas of flow sections after narrowing and before narrowing. We assume that $\zeta_1 = 0.5$, as $\omega_1 \to \infty$.

When turning the pipe, the value ζ_2 is determined as [21]:

$$\zeta_2 = 0.05 + 0.2\frac{d_{pp}}{R_{pp}} \tag{22}$$

where R_{pp} is bending radius of the pipeline (see Figure 4).

Local resistances during sudden expansion are determined by the Borda formula. Local resistances in the diffuser and confuser parts are determined according to [26].

Inertial head losses Δh_{in} consist of inertial head losses in stage 1 of the pump section in the connecting pipeline and in stage 2 $\Delta h_{in}=\Delta h_{in1}+\Delta h_{inpp}+\Delta h_{in2}$.

In stage 1 of the pump section and in the connecting pipeline, the determination of the inertial head losses does not depend on the direction of liquid movement. Their value can be defined as $\Delta h_{in1} = \frac{a_n}{g}z_1$; $\Delta h_{inpp} = \frac{a_{pp}}{g}l_{cpp}$.

We consider the inertial head losses in stage 2 of the PHPM.

When the liquid piston moves up:

- At $z_{2i} < S_1$ the inertial head losses are determined as:

$$\Delta h_{in2} = \frac{1}{g}\int_{R_1}^{R_i}\frac{a_i}{tg\alpha}dR \tag{23}$$

where $R_i = R_1 + z_{21} \cdot tg\alpha$; $a_i = \frac{F_1}{f_i}a_n - \frac{F_1v_1}{f_i^2}\omega\frac{df_i}{d\phi}$; $f_i = \pi R_i^2$.

- At $z_{2i} > S_1$

$$\Delta h_{in2} = \frac{1}{g}\int_{R_1}^{R_2}\frac{a_i}{tg\alpha}dR + \frac{1}{g}\int_{R_2}^{R_i}\frac{a_i}{tg\alpha}dR \tag{24}$$

where, $R_i = R_2 - z_{22} \cdot tg\alpha$.

When the piston moves down, Δh_{in2} is defined similarly.

3. Experimental Studies

The main purpose of the experiment is to check the performance of the two-stage PHPM, to gain new knowledge about its work, and to verify the developed mathematical model.

3.1. Subject of Research, Stand, and Measuring Equipment

A schematic diagram of a two-stage PHPM was previously shown in Figure 4. To exclude the influence of gas pulsations from the first stage, a 25 L receiver was additionally installed between the compressor stages.

The developed prototype of the two-stage PHPM had basic dimensions, Table 1.

Table 1. Main dimensions PHPM.

Indicator Description	Values
The diameter of the first stage piston	d_p = 0.050 m
Diameter of the rod of the first stage	d_r = 0.036 m
Full stroke of the 1st stage piston	S_h = 0.050 m
Initial coordinate of the liquid in the second stage	Z_{20} = 0.100 m
Diameter of the supply pipeline	d_{sp} = 0.016 m
The length of the supply pipeline	l_p = 0.5 m
Linear dead space	S_d = 0.0025 m
Turning radius of the supply pipeline	R_p = 0.5 m

The basic geometrical dimensions of the second stage are shown in Figure 5a.

The profiling of the working chamber of the second stage was carried out by installing the insert in the cylinder. The insert consisted of two cones connected at their vertices. Some accesses are made on the upper cone to ensure the passage of gas to the suction and discharge ports, and the base of the lower cone is made conical to improve the flow of liquid around it. The 3D view of the redesigned second stage is shown in Figure 5b. A photograph of the finished layout of the modernized second stage is shown in Figure 5c. Lobe valves were used as gas distribution bodies in the compressor section. To visualize the dynamics of the movement of the liquid piston, the second stage of the PHPM was made of Plexiglas, and the value of the discharge pressure was limited.

Table 2 shows the main dimensions of self-acting valves in stage 2 compressor section.
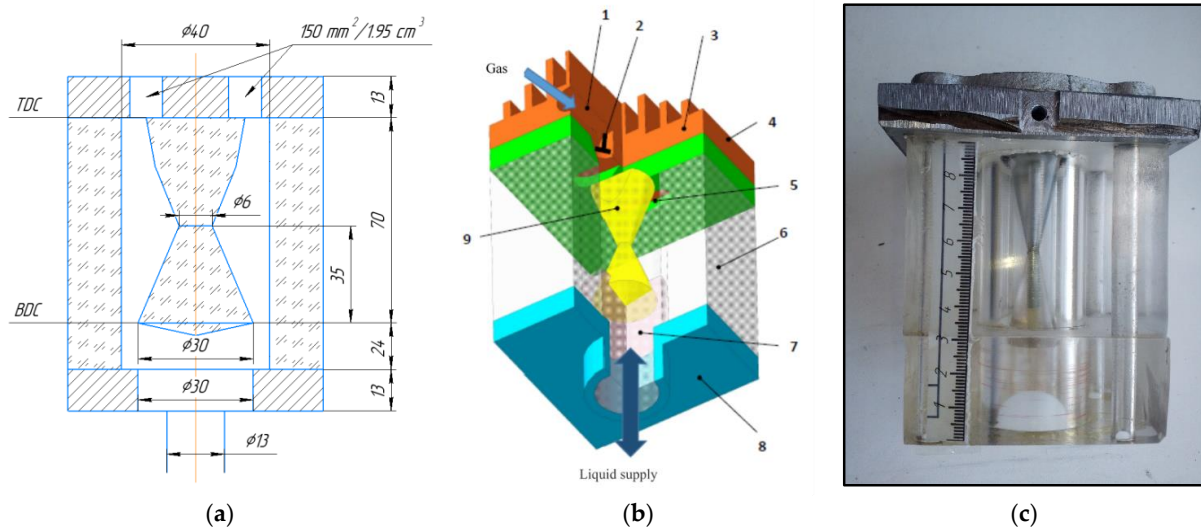

(a)   (b)   (c)

Figure 5. The profiling of the working chamber of the second stage: (**a**) Section of the working chamber of PHPM stage 2 with indication of the main size dimensions; (**b**) 3D image of the layout of the prototype of PHPM stage 2 (1. Suction line. 2. The suction valve of stage 2 of the compressor (shown conventionally). 3. Valve body. 4. Top flange. 5. Discharge window. 6. Plexiglas cylinder. 7. Liquid piston. 8. Bottom flange with tube. 9. Profiled insert); (**c**) Image of the PHPM stage 2 prototype.

Table 2. Size dimensions of self-acting valves of stage 2 compressor section.

Indicator Description	Values
Maximum lift height of the shut-off element of the suction valve in the compressor section	h_{scvmax} = 0.0015 m
The width of the passage in the seat of the suction valve of the compressor section	d_{scvc} = 0.023 m
Spring stiffness of the suction valve in the compressor section	c_{sscv} = 3200 N/m
Maximum lift height of the shut-off element of the discharge valve in the compressor section	h_{dvmax} = 0.0015 m
The width of the passage in the seat of the discharge valve of the compressor section	d_{dvc} = 0.023 m
Spring stiffness of the discharge valve in the compressor section	c_{sdv} = 3200 n/m

Working bodies used during experimental research are air, mineral oil (MGE-46V).

The prototype was tested on the developed stand; its general view is shown in Figure 6. A general view of the prototype installed on the stand is shown in Figure 7a. An image of the prototype on the stand is shown in Figure 7b.

To change smoothly the rotational speed of the drive shaft of the machine, a volumetric hydraulic drive is used, which includes a variable displacement axial piston pump model 313.3.56.804 with a discharge pressure 6.3 MPa and an axial piston hydraulic motor model 310.3.56.01.03.V.U.

Measurement of static pressures is performed by manometers, instantaneous pressures are measured with strain gauges.
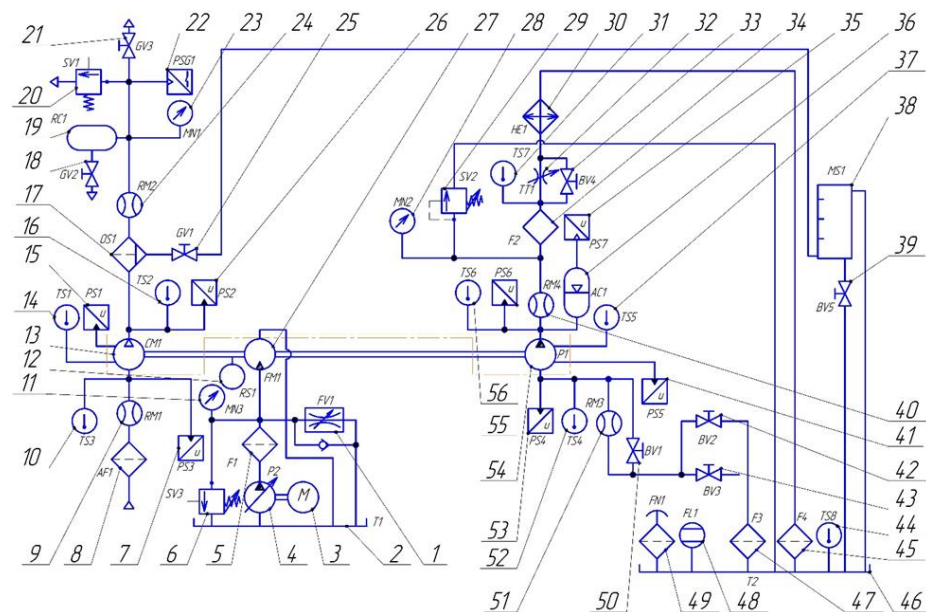

Figure 6. Hydropneumatic diagram of the experimental stand for two-stage PHPM studying. Legend: 1—fluid control valve; 2, 46—tank; 3—electromotor; 4, 54—pump; 5, 34, 45, 47—oil filter; 6, 20, 29—safety valve; 7, 15, 26, 35, 41, 55—pressure sensor; 8—air filter; 9, 24, 40, 51—ratemeter; 10, 14, 16, 31, 37, 44, 52, 56—temperature sensor; 11, 23, 28—manometer; 12—rotation sensor; 13—compressor; 17—oil-and-moisture separator; 18, 21, 25—globe valve; 19—receiver; 22—pressure switch gauge; 27—fluid-power motor; 30—heat exchanger; 32—throttle; 33, 39, 42, 43, 50—ball valve; 36—hydro-pneumatic accumulator; 38—measuring container; 48—fluid level gauge; 49—filler neck strainer; SV1-SV3—safety valve; GV1-GV3—globe valve; PSG1—pressure switch gauge; RC1—receiver; MN1-MN3—manometer; RM1-RM4—ratemeter; OS1—oil-and-moisture separator; TS1-TS8—temperature sensor; PS1-PS7—pressure sensor; CM1—compressor; AF1—air filter; F1-F4—oil filter; FN1—filler neck strainer; T1, T2—tank; P1, P2—pump; RS1—rotation sensor; FM1—fluid-power motor; FV1—fluid control valve; TT1—throttle; HE1—heat exchanger; BV1-BV5—ball valve; AC1—hydro-pneumatic accumulator; FL1—fluid level gauge; MC1—measuring container.

Suction and discharge temperatures are measured by TW-N PT100 sensors, the temperature of the liquid in the tanks is controlled by DTS-035-50M.B3 sensors.

The air flow rate at the suction of the first stage of the compressor is measured by the "Vector-04" model flow meters; we used the PSE530-M5-l sensors to measure the suction and discharge pressures.

The hydraulic and pneumatic lines of the stand are equipped with devices for liquid and gas purification, safety devices, and control equipment to operate the tested machine in different modes.

3.2. Verification of the Mathematical Model of Work Processes

One of the main tasks of the experimental research of the developed machine is to verify the mathematical model. The mathematical model verification was carried out at different values of the discharge pressure in stage 2, the suction pressure in stage 2 (discharge pressure in stage 1) and the crankshaft revolutions. An estimate of the experimental error and a comparison of the results of theoretical and experimental studies were published in [27].

It should be noted that the developed mathematical model describes the friction and inertia forces in moving liquid, as the data of indicator diagrams obtained experimentally and theoretically match; the maximum and minimum values of instantaneous pressures match as well.

Thus, the discrepancy in determining the instantaneous pressure in the machine cavities is within 10–15%.
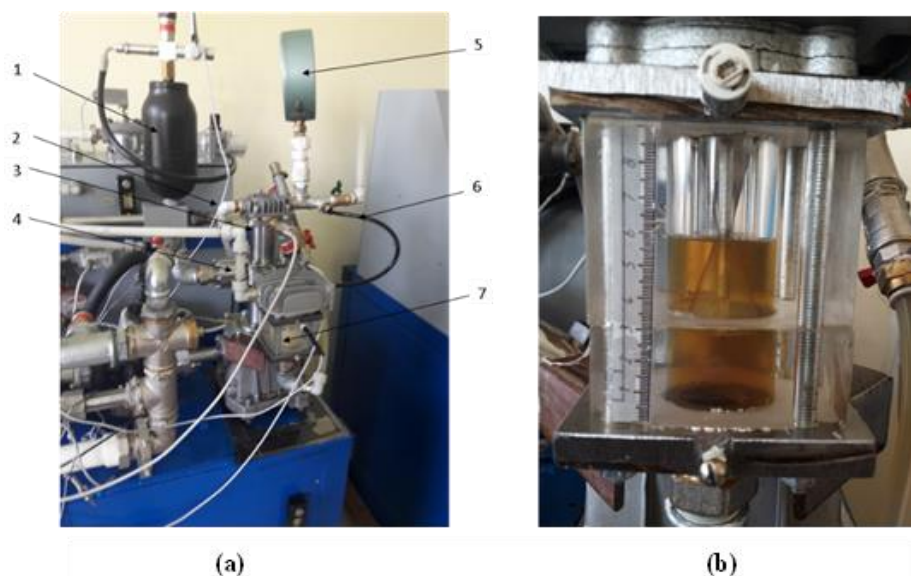

Figure 7. A general view of the prototype installed on the stand: (**a**) General view of two-stage PHPM with a gas cap (1—Gas cap; 2—Suction line; 3—Stage 1 of a two-stage PHPM; 4—Discharge line; 5—Manometer; 6—Inter -stage pipeline; 7—Stage 2 of two-staged PHPM); (**b**) Image of the prototype on the stand.

4. Results of a Numerical Experiment and Their Discussion

To carry out a numerical experiment, we choose a two-stage piston hybrid power machine with a profiled working chamber shown in Figure 8. The main geometrical and operational parameters are shown in Table 3.

As independent variables, we take the above-stated coefficient of dynamic viscosity and density of the liquid.

The dynamic viscosity coefficient varied from 0.0005 Pa to 0.04 Pa, and the density of the liquid varied from 600 kg/m^3 to 1400 kg/m^3.

Table 3. Main geometrical and operational parameters of two-stage PHPM.

| Indicator Description	Values
The diameter of stage 1 piston	$d_1 = 0.050$ m
Diameter of the stem of stage 1	$d_{st} = 0.036$ m
Full stroke of stage 1 piston	$S_{h1} = 0.050$ m
The number of revolutions of the crankshaft	$n_{rev} = 500$ rpm
Suction pressure	$P_{sc2} = 5 \times 10^5$ Pa
Discharge pressure	$P_{d2} = 25 \times 10^5$ Pa
The average temperature of the walls of the surface of the working chamber of stage 2	$\overline{T}_w = 330$ K
Intake air temperature	$T_{sc2} = 310$ K
Initial coordinate of the liquid in stage 2	$Z_{20} = 0.100$ m
Diameter of the supply pipeline	$d_{pp} = 0.016$ m
The length of the supply pipeline	$l_{pp} = 0.5$ m
Linear dead space	$S_{ds} = 0.0025$ m
Turning radius of the supply pipeline	$R_{pp} = 0.5$ m
The radius of the conical insert in the design scheme of stage 2 of the PHPM (see Figure 8)	$R_{21} = 0.003$ m, $R_{11} = 0.015$ m
The radii of the conical working chamber in the given design scheme of stage 2 of the PHPM:	$R_1 = 0.0132$ m, $R_2 = 0.01977$ m
The angle of inclination of the generatrix of the truncated cone	$\alpha = 0.235$ rad
Truncated cone height	$S_1 = 0.0272$ m
The maximum lifting height of the closure body of the discharge valve	$h_{dmax} = 0.001$ m
The maximum lifting height of the closure body of the suction valve	$h_{scmax} = 0.001$ m
The width of the passage in the saddle of the suction valve	$d_{scv} = 0.09$ m
The width of the passage in the saddle of the discharge valve	$d_{dv} = 0.09$ m
Spring rate of the discharge valve	$C_{sprd} = 16{,}280$ N/m
Spring rate of the suction valve	$C_{sprsc} = 5980$ N/m
Maximum clearance between the saddle and the closure body of the suction valve	$\delta_{sc} = 1 \times 10^{-8}$ m
Minimum clearance between the saddle and the closure body of the discharge valve	$\delta_d = 1 \times 10^{-8}$ m
Roughness of the inner surface of the connecting pipeline	$K = 0.000005$ m
Compressed gas	air
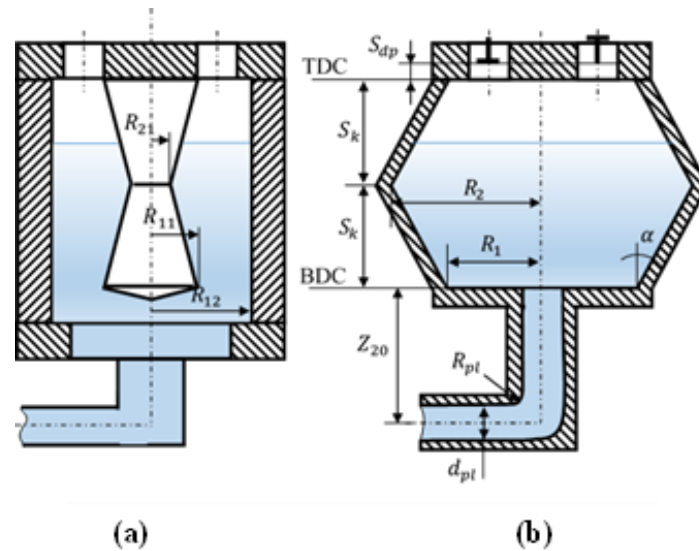
Figure 8. Two-stage piston hybrid power machine with a profiled working chamber: (**a**) objective design diagram of PHPM stage 2; (**b**) given design diagram of PHPM stage 2.

In carrying out the numerical experiment, we used the classical design with fractional replicas.

All response functions can be divided into two large groups. The first group is made up of functions that determine the flow of liquid in the machine: $\Delta \overline{p}_1 = \Delta p_1 / p_\Sigma$; $\Delta \overline{p}_2 = \Delta p_2 / p_\Sigma$; $\Delta \overline{p}_3 = p_3 / p_\Sigma$, where $\Delta p_\Sigma = \Delta p_1 + \Delta p_2 + \Delta p_3$; $\Delta p_1 = \int_0^{2\pi} |z_2 - z_1| \rho_w g \, d\varphi$; $\Delta p_2 = \int_0^{2\pi} \rho_w |(\alpha_2 V_2^2)/2 - (\alpha_1 V_1^2)/2| d\varphi$; $\Delta p_3 = \int_0^{2\pi} \rho_w g |\Delta h_l + \Delta h_\zeta + \Delta h_{in}| d\varphi$.

$\Delta \overline{p}_1$ determines the ratio of the geometric head to the sum of the geometric head, velocity head, and total head losses per cycle. $\Delta \overline{p}_2$ determines the ratio of the velocity head to the sum of the geometric head, velocity head, and total head losses per cycle. $\Delta \overline{p}_3$ determines the ratio of total head losses to the sum of geometric head, velocity head, and total head losses per cycle. $\Delta \overline{h}_l = \left(\int_0^{2\pi} |\Delta h_l| d\varphi \right) / \Delta h_\Sigma$–the ratio of head losses to hydraulic resistance along the length to the total head losses per cycle; $\Delta \overline{h}_\zeta = \left(\int_0^{2\pi} |\Delta h_\zeta| d\varphi \right) / h_\Sigma$–the ratio of head losses to local resistances to total head losses per cycle; $\Delta \overline{h}_{in_\Sigma} = \left(\int_0^{2\pi} |\Delta h_{in\Sigma}| d\varphi \right) / \Delta h_\Sigma$–ratio of inertial losses, taken in modulus, to total head losses per cycle, where $\Delta h_\Sigma = \int_0^{2\pi} \left(|\Delta h_l| + |\Delta h_\zeta| + |\Delta h_{in_\Sigma}| \right) d\varphi$.

The second group is made of functions determining the efficiency of stage 2 of the PHPM. Indicator work of the cycle in stage 2 is $L_{ind} = \oint V_2 dp$.

Technical work to overcome the frictional forces of the liquid in the machine $L_{fr} = \oint \rho_w g \left(|\Delta h_l| + |\Delta h_\zeta| \right) dV$.

The ratio of the work of friction forces to indicator work $\overline{L}_{fr} = L_{fr} / L_{ind}$.

Indicator isothermal efficiency of stage 2 of PHPM is:

$$\eta_{ind.is} = \frac{G_{cp} R T_{sc} \ln(p_d / p_{sc})}{L_{ind}} \tag{25}$$

Full indicator efficiency of stage 2 of PHPM:

$$\eta_{ind.f} = \frac{G_{cp} R T_{sc} \ln(p_d / p_{sc})}{L_{ind} + L_{fr}} \tag{26}$$

4.1. Analysis of the Influence of the Coefficient of Dynamic Viscosity

It should be noted that when analyzing the effect of liquid viscosity on the working processes of a two-stage PHPM, the total speed of liquid movement in the machine, including the pump section of the right-hand stage, the connecting pipeline and stage 2, as well as the liquid velocity only in the connecting pipeline, is of great importance, since it is the main source of hydraulic losses.

In the first case, the change in the total speed will be achieved by changing the angular speed of rotation, and in the second case—by changing the diameter of the connecting pipeline.

With a decrease in the dynamic viscosity coefficient μ_w at a constant density of the medium, the Reynolds number increases, the flow turbulization increases, leading to an increase in the hydraulic friction coefficient and an increase in the relative hydraulic losses along the length $\Delta \overline{h}_l$ and the value of the relative pressure losses per cycle $\Delta \overline{p}_3$ (see Figures 9 and 10).

It should be noted that a sharp increase in $\Delta \overline{h}_l$ and $\Delta \overline{p}_3$ is observed from the value of the coefficient of dynamic viscosity equal to 0.0008 Pa·s. Up to this value, we observe a linear drop in these values in the range of variation of μ_w from 0.02 Pa·s to 0.0008 Pa·s, which is fully consistent with the theory of laminar liquid motion. Against the sharp increase of $\Delta \overline{h}_l$ and $\Delta \overline{p}_3$, there is a sharp decrease in $\Delta \overline{p}_1$ and $\Delta \overline{h}_{in\Sigma}$ with a smooth decrease in $\Delta \overline{p}_2$.

In the range of μ_w variation from 0.02 Pa·s to 0.005 Pa·s, a decrease in the work of friction forces L_{fr} is observed and with a further decrease in μ_w the value L_{fr} increases (with a small local maximum) to 6.17 J, which is 14.89% (see Figure 11) from the indicator work of compression: the maximum value of the total indicator efficiency is 73.2% at μ_w = 0.005 Pa·s and its value drops to 64.2% at μ_w = 0.0005 Pa·s, i.e., by almost 10%. Values L_{ind} and $\eta_{ind.is}$ remain constant when changing μ_w.

Thus, the minimum L_{ind} and $\eta_{ind.f}$ does not coincide with the minimum $\Delta \overline{h}_l$ and $\Delta \overline{p}_3$ and is shifted towards large values of μ_w.
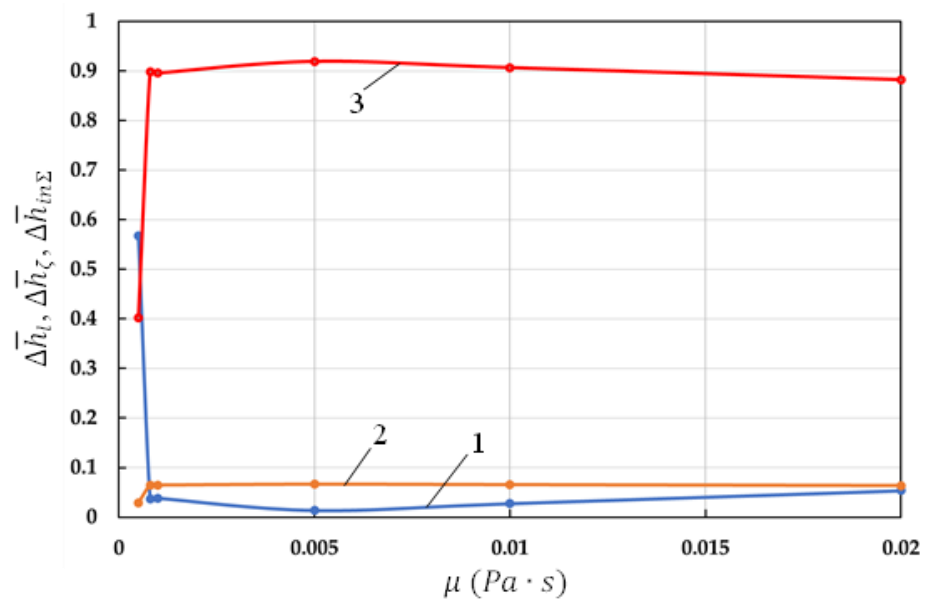
Figure 9. Dependence of the relative pressure losses along the length, to overcome local resistances and inertia forces on the dynamic viscosity coefficient (1-$\Delta \bar{h}_l$; 2-$\Delta \bar{h}_\zeta$; 3-$\Delta \bar{h}_{in\Sigma}$).
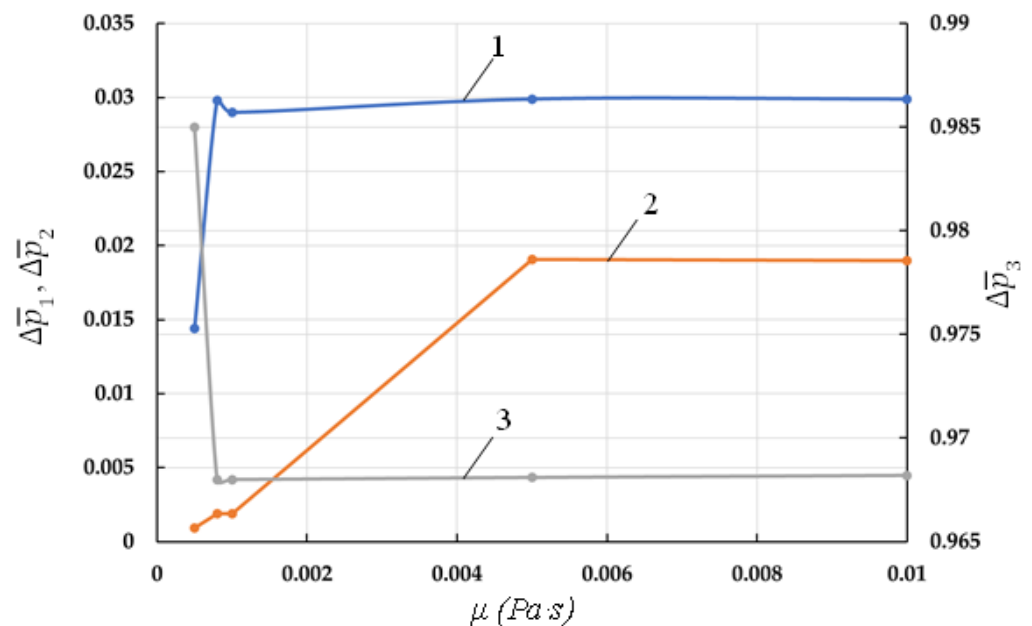

Figure 10. Dependence of relative pressure drops $\Delta \bar{p}_1$; $\Delta \bar{p}_2$; $\Delta \bar{p}_3$, on the dynamic viscosity coefficient (1-$\Delta \bar{p}_1$; 2-$\Delta \bar{p}_2$; 3-$\Delta \bar{p}_3$).

4.2. Influence of the Angular Velocity of the Crankshaft

With an increase in the angular velocity of the crankshaft, the speed of liquid movement in the stages of the machine and in the connecting pipeline increases. This leads to an increase in $\Delta \bar{p}_3$ and $\Delta \bar{h}_l$ while maintaining the previously described physical picture. The onset of flow turbulization and a sharp increase in the hydraulic friction coefficient along the length is shifted towards large values of μ_w.

Thus, if at $n_{rev} = 300$ rpm, minimum $\Delta \bar{h}_l$ is achieved at $\mu_w = 0.005$ Pa·s, then at $n_{rev} = 500$ rpm minimum $\Delta \bar{h}_l$ is achieved at $\mu_w = 0.010$ Pa·s, and at $n_{rev} = 750$ rpm minimum $\Delta \bar{h}_l$ is achieved at $\mu_w = 0.02$ Pa·s (see Figure 12).
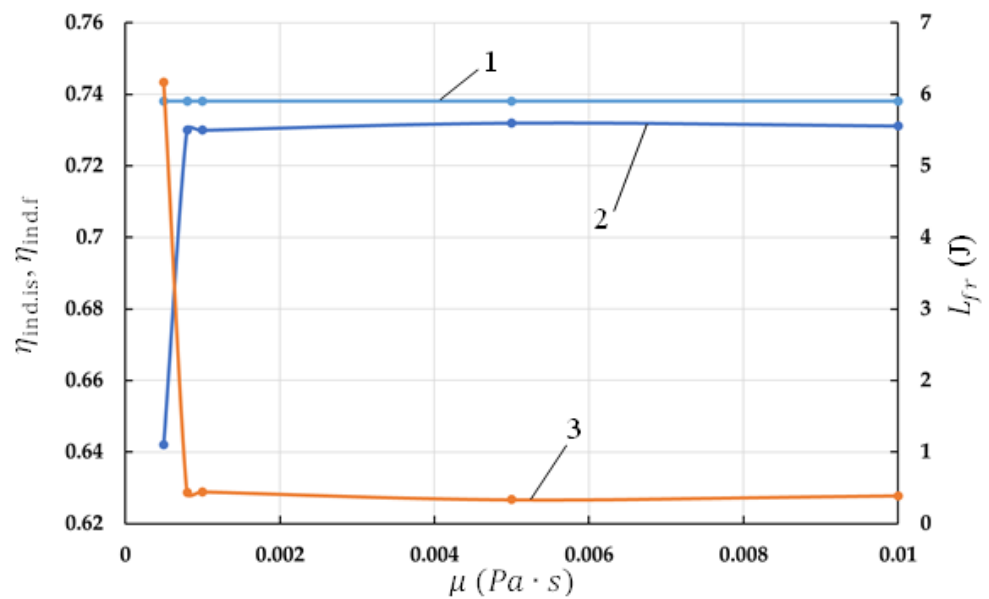
Figure 11. Dependence of indicator isothermal efficiency, total indicator efficiency and work of friction forces on the dynamic viscosity coefficient ($1\text{-}\eta_{ind.is}$; $2\text{-}\eta_{ind.f}$; $3\text{-}L_{fr}$).
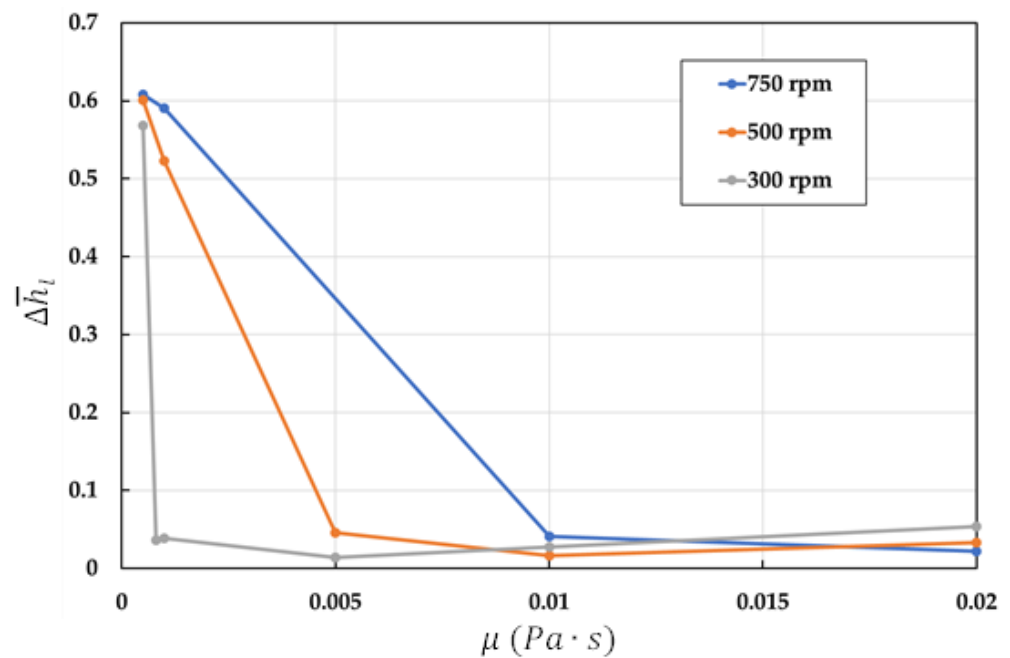

Figure 12. Dependence of the relative losses along the length on the coefficient of dynamic viscosity at different speeds of the crankshaft.

With an increase in n_{rev} and an increase in $\Delta\bar{h}_l$ there is an increase in L_{fr} and the total indicator efficiency decreases. Maximum $\eta_{ind.f}$ shifts towards larger values of μ_w while simultaneously decreasing it in absolute terms. The maximum $\eta_{ind.f}$ and minimum L_{fr} points coincide with the minimum points $\Delta\bar{h}_l$. Absolute decrease in the maximum value of the indicator efficiency is 0.041 or 5.93%.

It should be noted that at the number of revolutions $n_{rev} = 750$ rpm and $\mu_w = 0.0005$ Pa·s, the value of the work of the friction forces L_{fr} slightly exceeds the work for gas compression in the second stage of the machine $L_{ind.is}$ and $\eta_{ind.f}$ drops to 0.362, i.e., decreases by almost half.

4.3. Influence of the Diameter of the Connecting Pipe

It should be noted that the connecting pipeline is of decisive importance in the balance of total hydraulic losses along the length. This led to its consideration.

A change in the diameter of the connecting pipeline leads to a change in the speed in it and, therefore, the physical picture of working processes and changes in energy characteristics will be similar to that considered. As a result, we consider the working processes of the machine under study and its energy characteristics at constant μ_w and n_{rev} and a variable value of the pipeline diameter (d_{pp}).

With an increase in the diameter of the pipeline (d_{pp}), velocity of the liquid in it decreases, which leads to a decrease in the hydraulic resistance and an increase in $\Delta \bar{p}_3$ with a simultaneous increase in $\Delta \bar{p}_1$ and $\Delta \bar{p}_2$.

It should be noted that when d_{pp} changes from 0.014 m to 0.022 m, there is a linear drop in $\Delta \bar{p}_3$ from 0.9924 to 0.981 (see Figure 13).
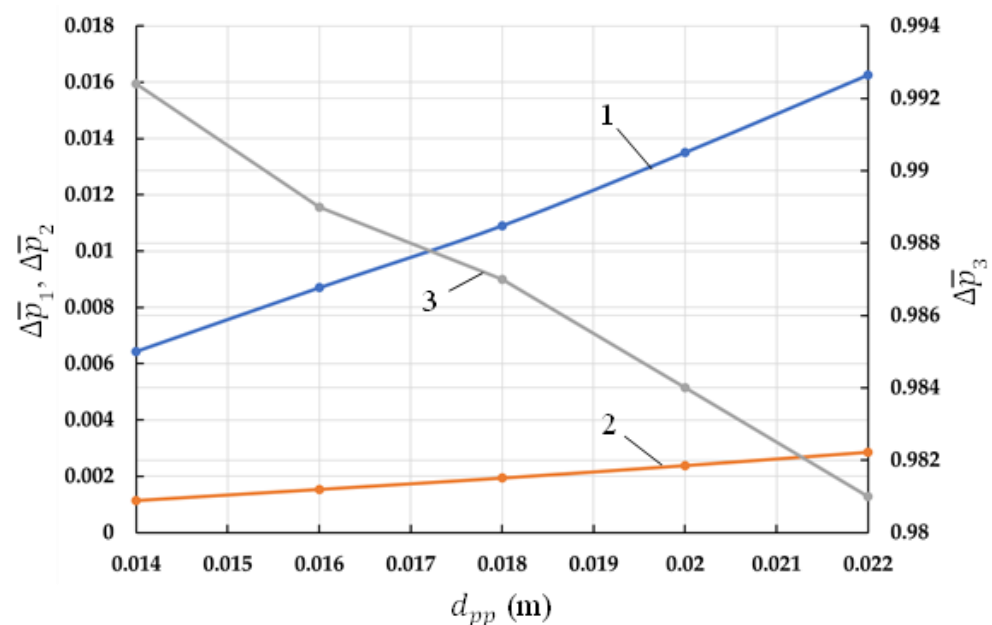

Figure 13. Dependence of relative pressure loss $\Delta \bar{p}_1$; $\Delta \bar{p}_2$; $\Delta \bar{p}_3$, on the diameter of the supply pipeline (1-$\Delta \bar{p}_1$; 2-$\Delta \bar{p}_2$; 3-$\Delta \bar{p}_3$).

With a decrease in d_{pp}, there is a drop in $\Delta \bar{h}_l$ and $\Delta \bar{h}_\zeta$ with an increase in the relative inertial losses $\Delta \bar{h}_{in\Sigma}$. The curve $\bar{h}_l = f(d_{pp})$ has a parabolic character with a sharp increase with decreasing d_{pp}, but the curve $\bar{h}_\zeta = f(d_{pp})$ is close to linear (see Figure 14).

With an increase in d_{pp} and a decrease in hydraulic losses along the length and on local resistances there is a decrease in the work of friction forces L_{fr} and an increase in the total indicator efficiency. With an increase in d_{pp}, the value L_{fr}/L_{compr} decreases from 8.8% to 1%, when increasing d_{pp} from 0.014 m to 0.022 m, but the value of the total indicator efficiency increases from 0.674 to 0.726, i.e., more than 0.05, which is almost 10%.

4.4. Analysis of the Effect of Liquid Density

To analyze the influence of the density of the coolant on the working processes and characteristics of the machine, we take: d_{pp} = 0.018 m; n_{rev} = 500 rpm; μ_w = 0.01 Pa·s.

With a change in ρ_w values $\Delta \bar{p}_1$ and $\Delta \bar{p}_2$ have maximum at ρ_w = 1200 kg/m³, although these maxima are negligible and can be neglected, which allows us to conclude that $\Delta \bar{p}_1$, $\Delta \bar{p}_2$, and $\Delta \bar{p}_3$ remain constant when ρ_w change in the range from 600 kg/m³ to 1400 kg/m³.

In the range of density variation, we observe a minimum of $\bar{h}_l$ at ρ_w = 1200 kg/m³ and maximum $\bar{h}_l$. It should be noted that $\Delta \bar{h}_\zeta$ changes insignificantly, while $\bar{h}_l$ decreases almost twofold. The influence of the density of the working fluid is very complicated.

With a change in density, the Re number changes at a constant μ_w, which leads to a change in the value of the coefficient of friction along the length, and the values of the hydrostatic and velocity heads change. The maximum relative inertial losses are achieved at $\rho_w =1200$ kg/m^3 and make up the biggest share of the total inertial losses—92%.

With an increase in the density of the liquid the work of friction forces L_{fr} increases almost linearly from $\rho_w =600$ kg/m^3 to 1100 kg/m^3, with a further increase in ρ_w the value L_{fr} changes parabolically (see Figure 15). With a decrease in density due to the fact that L_{fr} decreases, there is an increase in the total indicator efficiency. Its value increases from 0.7036 at $\rho_w = 1400$ kg/m^3 to 0.722 at $\rho_w = 600$ kg/m^3, i.e., by almost 2% (see Figure 15).

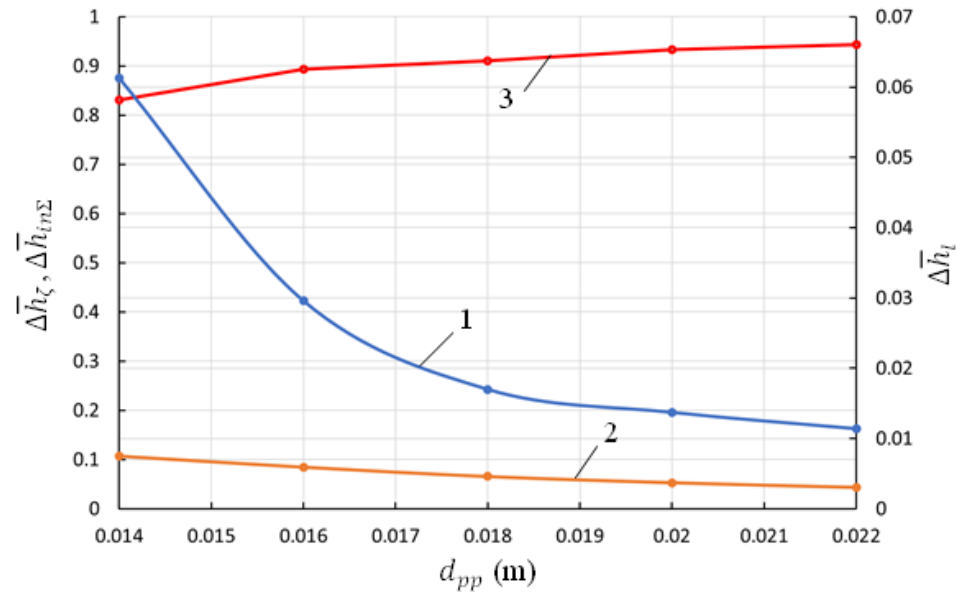**Figure 14.** Dependence of the relative head losses along the length to overcome local resistances and inertial forces on the diameter of the supply pipeline (1-$\Delta \bar{h}_l$; 2-$\Delta \bar{h}_\zeta$; 3-$\Delta \bar{h}_{in\Sigma}$).
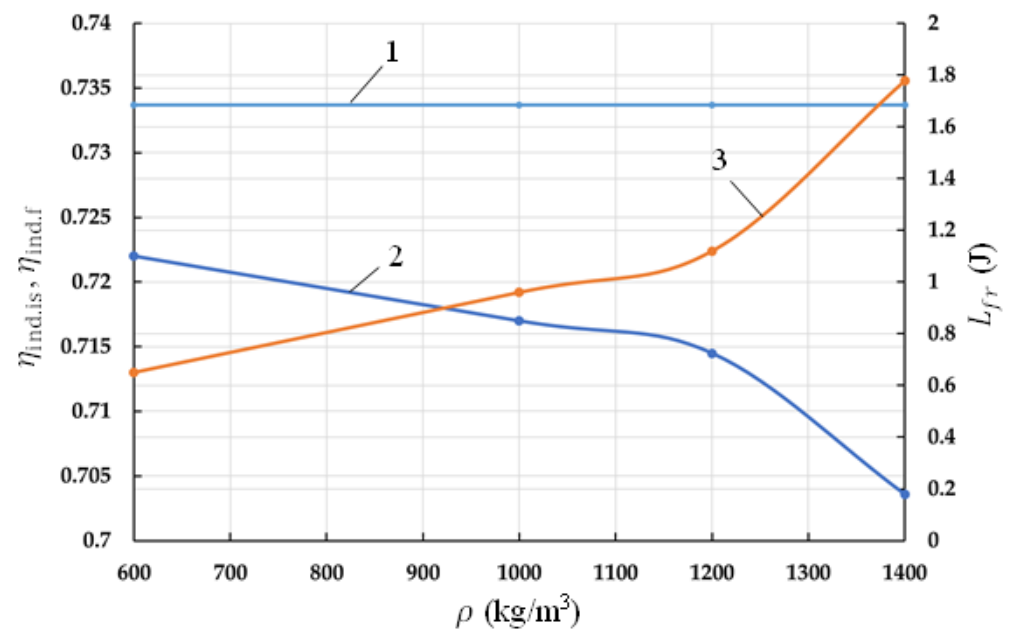

Figure 15. Dependence of the indicator isothermal efficiency, total indicator efficiency, and work of friction forces on the liquid density (1-$\eta_{ind.is}$; 2-$\eta_{ind.f.}$; 3-L_{fr}).

5. Conclusions

In the manuscript, a mathematical model of the working processes of a two-stage piston hybrid power machine designed to compress gas to medium and high pressures has been developed and validated. A numerical experiment was carried out to study the influence of the viscosity and density of the working fluid on the working processes in the machine under study.

As a result of the numerical experiment, we determined:

(1) There is a value of the optimal value μ_w, which provides the maximum value of the total indicator efficiency and bypassing the work of the forces of liquid friction. The optimal μ_w is in the range from 0.005 Pa·s to 0.02 Pa·s, with a change in the number of revolutions of the crankshaft from 300 rpm to 750 rpm.

(2) With an increase in the angular velocity of the crankshaft to obtain maximum efficiency, it is necessary to increase the dynamic viscosity coefficient. The use of water as a coolant is not effective, because as the temperature rises, it decreases and at the operating temperature T = 323 K; its value is μ_w = 0.0005494 Pa·s, which corresponds to the minimum indicator efficiency and the maximum work of friction forces. An increase in the diameter of the connecting pipeline leads to a decrease in the work of friction forces and an increase in the indicator efficiency.

(3) With a decrease in the density of the medium, the total indicator isothermal efficiency increases and the work of friction forces L_{fr} decreases. The minimum relative hydraulic losses along the length and the maximum $\Delta \bar{p}_1$ and $\Delta \bar{p}_2$ correspond to ρ_w = 1200 kg/m^3.

(4) The analysis showed that industrial oil I-12A, which has ρ_w = 880 kg/m^3 and μ_w/ρ_w = (13÷17)·10^{-6} m^2/s can be used as power liquid in the machines.

Author Contributions: Conceptualization, V.S. and E.N.; methodology, V.S.; software, E.P.; validation, V.S. and E.P.; formal analysis, V.S.; investigation, V.S., E.P., E.N., and I.B.; writing—original draft preparation, V.S. and I.B.; writing—review and editing, I.B. and E.P.; visualization, E.P. and E.N.; supervision, V.S.; project administration, V.S. All authors have read and agreed to the published version of the manuscript.

Informed Consent Statement: Not applicable.

Conflicts of Interest: The authors declare no conflict of interest.

Nomenclature

The nomenclature of the paper is shown below:

α	angle between the generatrix of the cone and the height;
α_1	coriolis coefficient for Section 1;
α_2	coriolis coefficient for Section 2;
α_w	heat transfer coefficient of compressible gas;
β_p	coefficient of volume compressibility;
α_w	coefficient of temperature expansion;
β_p	head loss due to inertial resistance in stage 1 of the pump section;
β_T	head loss due to inertial resistance in the working chamber of stage 2;
Δh_{in1}	head loss due to inertial resistance in the pipeline;
Δh_{in2}	head loss along the length in the cylinder of stage 1 pumping section;
Δh_{inpp}	head loss along the length in the working chamber of stage 2;
Δh_{l1}	head loss along the length in connecting pipeline 3;
Δh_{l2}	pressure loss in the interstage connecting of the compressor section;
Δh_{lpp}	undercooling value of gas sucked into stage 2 of the compressor section;
Δp_c	the ratio of the discharge pressure to the suction pressure of stage 1;
ΔT_{H0}	flow rates in stages 1 of the compressor section;
ε_1	flow rates in stages 2 of the compressor section;

λ_1 ratio of piston stroke to twice the length of the connecting rod;

λ_2 coefficient of friction along the length in the cylinder of stage 1;

λ_m coefficient of friction along the length in the working chamber of stage 2;

λ_{c1} coefficient of friction along the length in the connecting pipe;

λ_{c2} dynamic viscosity;

λ_{cpp} liquid density;

μ_w sum of forces acting on the valve closure;

ρ_w crankshaft angle;

ΣF_i piston acceleration;

φ acceleration in the connecting pipeline;

a_n stage 1 cylinder diameter;

a_{pp} elementary time interval;

d_1 connecting pipe diameter;

$d\tau$ elementary *i:th* separable mass of gas;

d_{pp} elementary *i:th* attached mass of gas;

dM_{0i} rod diameter in PHPM stage 1;

dM_{ni} elementary heat input;

d_r stage 1 mechanical piston area;

dQ_g working chamber lateral surface area;

F_1 heat exchange surface;

F_b piston surface area;

F_{ni} valve plate area;

F_p cross-sectional area;

F_{vp} gravity acceleration;

f_w mass of gas supplied to the discharge line;

g head loss on local resistance;

G_{cp} degree of valve closure lift;

h_ζ inertial head losses;

h_c head loss along the length;

h_{in} specific enthalpy of the separated gas mass;

h_l specific enthalpy of the added *i:th* mass of gas;

i_0 adiabatic exponent;

i_{ni} connecting pipe length;

k reduced mass of the self-acting valve closure;

l_{cpp} number of sources of separated and attached gas masses;

m_{rdv} pressure in stage 1 of discharge chamber;

N_1, N_2 gas pressure;

p_{D1} gas pressure at the suction of stage 1 of the compressor section;

p_g gas pressure at the suction of stage 2 of the compressor section;

p_{sc1} liquid pressure;

p_{sc2} liquid flow;

p_w small radius of the truncated cone;

Q_w large truncated cone radius;

R_1 truncated cone height;

R_2 piston stroke;

S_1 piston stroke in PHPM stage 1;

S_h linear dead space;

S_{h1} average integral temperature of the lateral surface of the working chamber;

S_{ld} temperature of the compressible gas;

$\overline{T}_b$ suction gas temperature in stage 1 of the compressor section;

T_g suction gas temperature in stage 2 of the compressor section;

T_{sc1} mean integral temperature of the valve plate surface;

T_{sc2} mean integral temperature of the surface of the compression chamber;

$\overline{T}_{vp}$ total internal energy of the compressible gas;

$\overline{T}_w$ mechanical piston speed in stage 1 pumping section;

U_g gas volume;

V_1 the working volume of the pumping section of stage 1;

V_g working volume of stage 1 of the compressor section;

V_{cp1} working volume of stage 2 of the compressor section;

V_{h1}	liquid velocity in the connecting line;
V_{h2}	suction gas volume in stage 1 of the compressor section;
V_{pp}	suction gas volume in stage 2 of the compressor section;
V_{sc1}	liquid velocity;
V_{sc2}	coordinate of the gravity center of the first cross-section;
V_w	coordinate of the gravity center of the second cross-section;
z_1	distance from the axis of connecting pipeline 3 to the lower surface of the working chamber of stage 2;
z_2	coordinate of the surface of the liquid piston;
z_{20}	distance from the surface of O-O cross-section to the surface of the liquid piston;
z_{21}	the coordinate of the gravity centers of the cross-sections;

References

1. Abdel-Hadi, A.; Salem, A.R.; Abbas, A.I.; Qandil, M.; Amano, R.S. Study of energy saving analysis for different industries. *J. Energy Resour. Technol. Trans. ASME* **2021**, *143*, 052101. [CrossRef]
2. Silva, E.; Dutra, T. Piston trajectory optimization of a reciprocating compressor. *Int. J. Refrig.* **2021**, *121*, 159–167. [CrossRef]
3. Yan, B.; Wieberdink, J.; Shirazi, F.; Li, P.Y.; Simon, T.W.; Van de Ven, J.D. Experimental study of heat transfer enhancement in a liquid piston compressor/expander using porous media inserts. *Appl. Energy* **2015**, *154*, 40–50. [CrossRef]
4. Dindorf, R. Estimating Potential Energy Savings in Compressed Air Systems. *Procedia Eng.* **2012**, *39*, 1877–7058. [CrossRef]
5. Ueno, K.; Hunter, K.S. *Compressor Efficiency Definitions*; University of Colorado: Boulder, CO, USA, 2003.
6. Shcherba, V.E.; Paramonov, A.M.; Blinov, V.N.; Surikov, V.I.; Nosov, E.Y.; Tegzhanov, A.S. Comparative analysis of process of cooling of compressible gas in crosshead and crossheadless hybrid positive-displacement piston power machines. *Chem. Pet. Eng.* **2020**, *55*, 733–742. [CrossRef]
7. Seshaiah, N.; Sahoo, R.K.; Sarangi, S.K. Theoretical and experimental studies on oil injected twin-screw air compressor when compressing different light and heavy gases. *Appl. Therm. Eng.* **2010**, *30*, 327–339. [CrossRef]
8. Vittorini, D.; Cipollone, R. Energy saving potential in existing industrial compressors. *Energy* **2016**, *102*, 502–515. [CrossRef]
9. Qv, D.; Dong, B.; Cao, L.; Ni, L.; Wang, J.; Shang, R.; Yao, Y. An experimental and theoretical study on an injection-assisted air-conditioner using R32 in the refrigeration cycle. *Appl. Energy* **2017**, *185*, 791–804. [CrossRef]
10. Wang, X.; Hwang, Y.; Radermacher, R. Two-stage heat pump system with vapor-injected scroll compressor using R410A as a refrigerant. *Int. J. Refrig.* **2009**, *32*, 1442–1451. [CrossRef]
11. Plastinin, P.I. *Reciprocating Compressors*; Tom 1: Moscow, Russia, 2006; 456p.
12. Shcherba, V.E.; Bolshtyanskii, A.P.; Kaigorodov, S.Y.; Kuzeeva, D.A. Benefits of Integrating Displacement Pumps and Compressors. *Russ. Eng. Res.* **2016**, *36*, 174–178. [CrossRef]
13. Zhang, C.; Li, P.Y.; van de Ven James, D. Design analysis of a liquid-piston compression chamber with application to compressed air energy storage. *Appl. Therm. Eng.* **2016**, *101*, 704–709. [CrossRef]
14. Patil, V.C.; Acharya, P.; Ro, P.I. Experimental investigation of heat transfer in liquid piston compressor. *Appl. Therm. Eng.* **2019**, *146*, 169–179. [CrossRef]
15. ToroK, A.; Petrescu, S.; Popescu, G. Quasi-Izothermal Compressors and Expanders with Liquid Piston. Available online: https://hal.archives-ouvertes.fr/hal-02461111/document (accessed on 16 January 2022).
16. Piya, C.; Sircar, I.; Van de Ven James, D.; Olinger, D.J. Numerical Modeling of Liquid Piston Gas Compression. In Proceedings of the ASME International Mechanical Engineering Congress and Exposition, Lake Buena Vista, FL, USA, 13–19 November 2009; pp. 507–517.
17. Kermani, N.A.; Rokni, M. Heat transfer analysis of liquid piston compressor for hydrogen applications. *Int. J. Hydrog. Energy* **2015**, *40*, 11522–11529. [CrossRef]
18. Zhang, C.; Yan, B.; Wieberdink, J. Thermal analysis of a compressor for application to compressed air energy storage. *Appl. Therm. Eng.* **2014**, *73*, 1402–1411. [CrossRef]
19. Saadat, M.; Li, P.Y.; Sirnon, T.W. Optimal trajectories for a liqu.id piston compressor/expander in a compressed air energy storage system with consideration of heat transfer and friction. In Proceedings of the American Control Conference (ACC), Montréal, QC, Canada, 27–29 June 2012; IEEE: Piscataway, NJ, USA, 2012; pp. 1800–1805.
20. Shcherba, V.E.; Zanin, A.V.; Khrapskii, S.F. Fluid motion dynamics in a two-stage piston hybrid power machine. *Chem. Pet. Eng.* **2020**, *56*, 534–542. [CrossRef]
21. Shcherba, V.E.; Shalai, V.V.; Pustovoi, N.; Zanin, A.V. On Profiling of the Working Cavity of the Second Stage in a Hybrid Piston Volumetric Power Machine. *Chem. Pet. Eng.* **2020**, *56*, 125–136. [CrossRef]
22. Vimmr, J. Mathematical modelling of compressible inviscid fluid flow through a sealing gap in the screw compressor. *Math. Comput. Simul.* **2003**, *61*, 187–197. [CrossRef]
23. James, D.; Van de Ven Perry, Y.L. Liquid piston gas compression. *Appl. Energy* **2009**, *86*, 2183–2191. [CrossRef]
24. Xu, W.; Du, Z.; Wang, X.; Cai, M.; Jia, G.; Shi, Y. Isothermal piston gas compression for compressed air energy storage. *Int. J. Heat Mass Transf.* **2020**, *155*, 119779. [CrossRef]

25. Bradshaw, C.R.; Groll, E.A.; Garimella, S.V. A comprehensive model of a miniature-scale linear compressor for electronics cooling. *Int. J. Refrig.* **2011**, *34*, 63–73. [CrossRef]
26. Kundu, P.K.; Cohen, I.M.; Dowling, D.R. *Fluid Mechanics*; Academic Press: London, UK, 2015.
27. Zanin, A.; Pavlyuchenko, E.A.; Shcherba, V.E. Numerical and experimental study on fluid compressibility in a two-stage reciprocating pump-compressor. *Appl. Therm. Eng.* **2021**, *194*, 117106. [CrossRef]